Distinct outputs of CDC-42 combine to activate and brake contractility in M-phase *C. elegans* embryos

Authors and order

March 19, 2024

1 The distinction between establishment and maintenance

Figure we want to make for this section:

(a) ?

(A) Cell cycle progression controls a regime change from rho-dependent contractility to CDC-dependent contractility.

(B) Relaxation of pseudo-cleavage is a marker for this transition (so is onset of centration).

(C) CDC-42 also involved in biochemistry (complexing with PAR-6/PKC-3 to inhibit pPARs), so biochemistry and contractility are intimately coupled in maintenance phase (different from establishment phase where rho has its own pulsatile/oscillatory dynamics).

2 The steady state of maintenance phase

It has been previously observed that embryos in late-maintenance phase exhibit a steady pattern of anterior-directed cortical flow (see [12, Fig. 2]). Yet, despite the anterior-directed contractility, the A/P boundary in late maintenance appears to be stable. It remains unclear if this pattern of flow is a consequence of establishment-phase patterning of myosin [9], or if the pattern of flow is merely transient and would eventually stop if the cell cycle extended long enough. In this section, we establish that the pattern of flow and myosin profile in maintenance phase are in fact robust (to changes in establishment phase contractility) and long-lasting (if maintenance phase is extended);

in other words, we seek to show that maintenance-phase biochemistry encodes an attractive steady state.

Figure we want to make for this section:

(a) Kymograph showing rescue
(b) Pictures of myosin distribution in early and late maintenance in wild type and ts ect-2
(c) Fig. 1 in this report (showing progression of myosin and flow over time)
(d) Kymograph from MRCK (RNAi) experiment showing failure of rescue
(e) Kymograph from CDK-1 experiment showing boundary is stable
(f) We will not show messy flows and myosin (from CDK-1) but put those in SI

2.1 Maintenance-phase rescue

In addition to stabilizing asymmetries that are set up during establishment phase, the biochemical and mechanical interactions in maintenance phase can also rescue a steady polarized state. While this has been observed in previous studies in *ect-2* mutants [14, 13], which cannot activate Rho and consequently lack myosin functionality during establishment phase, it has yet to be shown that the steady polarized state that results is the same as in wild-type embryos. To establish this, we systematically image rescue of symmetry breaking in temperature-sensitive *ect-2* mutants, marking the beginning of maintenance phase via the transition of myosin from large to small clusters, and the end of maintenance phase as the onset of embryo rotation prior to cytokinesis. This gives a roughly four minute window of maintenance phase for each embryo, in which we track the average myosin intensity profile and flow speed.

In Fig. 1 we show the myosin intensity and flow speed over 30 second intervals of maintenance phase rescue, and compare the result to the steady myosin intensities and flow speeds observed in wild-type embryos [12]. The myosin peak initially grows in size advances rapidly towards the anterior, but after about three minutes it stops growing and becomes pinned at about 40% embryo length. The pinning of the myosin peak corresponds to a decrease in the maximum flow speed from about 4.5 μm/min (from 2:00 to 3:30) to 2 μm/min in the last 30 seconds of maintenance phase (3:30 to 4:00, see the inset of Fig. 1). In the last 30 seconds of maintenance phase, the flow profile in *ts ect-2* embryos is roughly the same as that observed during late maintenance phase in wild-type embryos. The myosin intensity appears quantitatively different, but has the same fundamental shape: there is a gradient of myosin in both the anterior and posterior, with a maximum occurring at around 40% of the embryo length. These results establish that the biochemical circuit governing maintenance phase can amplify small residual asymmetries from establishment phase, and that the

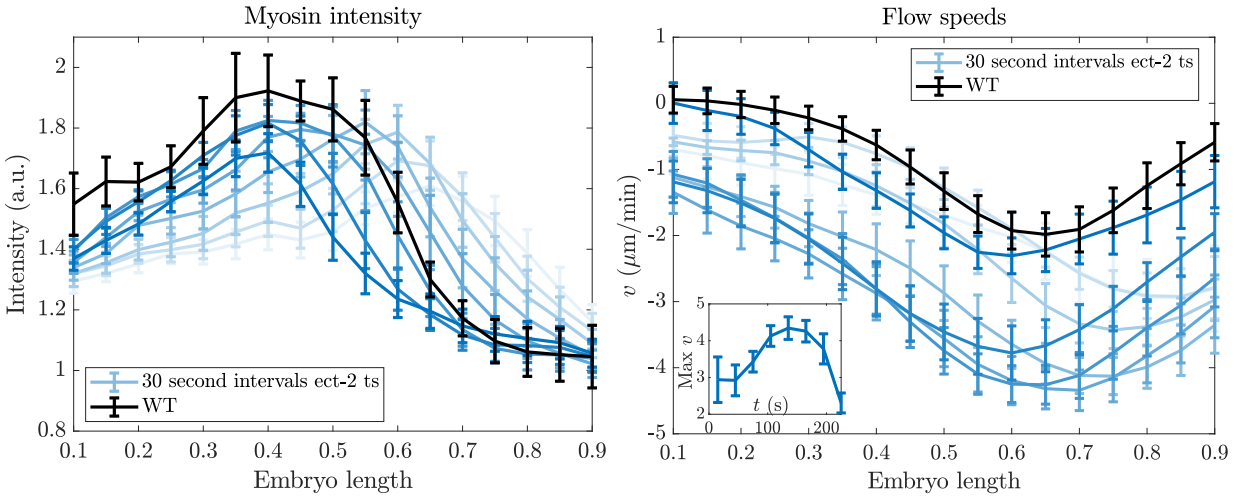

Figure 1: Comparing the end of maintenance phase in *ts ect-2* mutants to wild-type embryos. Left panel: myosin intensity profile. Right panel: flow speeds (inset shows the maximum flow speed over time). The blue colored lines show 30-second intervals of maintenance phase in *ts ect-2* embryos, with darker blue denoting later times. The black line shows the profile extracted from the last minute of maintenance phase in wild type embryos [12].

resulting polarized state is independent of what comes before maintenance.

2.1.1 Rescue requires MRCK

Need to show that it cannot happen without myosin flows.

2.2 Extending maintenance phase establishes

The pinning of the myosin boundary and subsequent decrease in the speed of flow hint that the cell has a built-in mechanism to prevent the boundary from contracting off the end of the embryo. But is it really possible to maintain a steady myosin intensity profile in the presence of a persistently anterior-directed flow?

To probe whether the myosin intensity and patterns of flow we see in late maintenance phase are truly steady states, we extend maintenance phase by treating wild-type embryos with CDK-1 (RNAi). Marking the start of maintenance phase by the end of pseudo-cleavage, and the end of maintenance phase by the onset of cytokinesis, we obtain a window of roughly 8–10 minutes per cell, in which we characterize the myosin intensity and flow speeds (see SI). Later stages of the extended maintenance show a relatively stable position of the myosin boundary (it in fact expands towards the posterior slightly) and a persistent anterior-directed flow which tends to achieve a

maximum (magnitude) just posterior of the peak myosin location. Because the myosin intensity and flow speeds in *CDK-1* (RNAi) never resemble those of wild-type, it is clear that interfering with CDK-1 affects more than just the cell cycle, and it is impossible to say concretely that the specific flow and myosin profiles in late maintenance are "steady." Nevertheless, we can say definitively that a persistent anterior-directed flow does *not* lead to further contraction of the boundary when maintenance is extended.

3 Model reveals existing mechanisms cannot explain rescue

Our goal in this section is to explore existing literature mechanisms for how maintenance phase biochemistry could set an attractive steady state. At first glance, it appears that the phenomenon of maintenance phase rescue is a consequence of an instability of the underlying system; a small perturbation in the myosin concentration could induce an anterior-directed flow, which drives the system to the polarized state. Here we systematically exclude this by considering a model of myosin alone and showing that spontaneous symmetry breaking is not possible with realistic parameters. We then consider PAR proteins, showing that, while the PAR circuit we consider can maintain a stable polarized state with a fixed boundary position, the time required to set up this state is prohibitively long, and myosin-directed flows are required. Finally, we consider a combination of myosin-driven flows *and* PAR proteins. This model allows us to reproduce the initial stages of maintenance phase rescue, but it cannot explain the sudden slow-down in flow speeds and pinning of the myosin boundary.

Figure we want to make for this section:

(a) Stability analysis for myosin (Fig. 2 here)
(b) Schematic of biochemistry model (Fig. 3 here)
(c) Cytoplasmic depletion with PARs (Fig. 4 here)
(d) Attempt at rescue with myosin (Fig. 5 here)

3.1 Myosin without additional feedback cannot spontaneously polarize

We first explore the dynamics of myosin alone, which we describe in terms of a one-dimensional spatially and temporally varying field $M(x,t)$ which evolves according to the advection-diffusion-

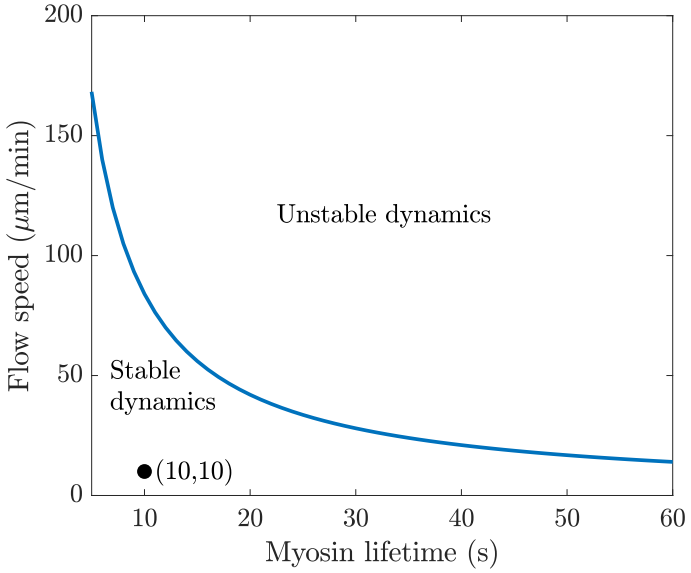

Figure 2: Required flow speeds for spontaneous polarization of myosin during maintenance phase. We plot $v = \ell/\tau_M$, where $\tau_m = 1/k_M^{\text{off}}$ is the myosin lifetime and $\ell = 14$ μm is the hydrodynamic lengthscale. Flow speeds above the blue line give unstable dynamics, while flow speeds below it give stable dynamics.

reaction equations [1]

$$\partial_t M + \partial_x (vM) = D_M \partial_x^2 M + k_M^{\text{on}} M_{\text{cyto}} - k_M^{\text{off}} M \tag{1a}$$

$$\gamma v = \eta \partial_x^2 v + \partial_x \sigma_a(M) \tag{1b}$$

The velocity field (1b) comes from the assumption that myosin generates an active stress $\sigma_a(M)$, which combines with the viscous stress to give the total cortical stress $\sigma = \eta \partial_x v + \sigma_a(M)$. The force balance equation in the fluid says that the force due to stress must be balanced by the drag force, $\gamma v = \partial_x \sigma$, where γ is the drag coefficient. Combining the force balance with the stress expression gives the velocity equation (1b), which can also be rewritten in terms of the "hydrodynamic lengthscale" $\ell = \sqrt{\eta/\gamma} \approx 14$ μm, which is essentially the lengthscale on which a local increase in the myosin field will pull in neighboring molecules [6]. As in [1], we ignore the elastic part of the stress, since the actomyosin cortex is purely viscous on timescales longer than the cortical turnover time [6].

In the case when diffusion of myosin is negligible and all myosin is bound to the membrane, the stability analysis in the SI shows that the dynamics are unstable when the flow carries myosin molecules a distance larger than the hydrodynamic lengthscale, i.e., $v/k_M^{\text{off}} > \ell$. Substituting $\ell \approx 14$ μm, we plot the velocity threshold for instability as a function of myosin lifetime in Fig. 2. For

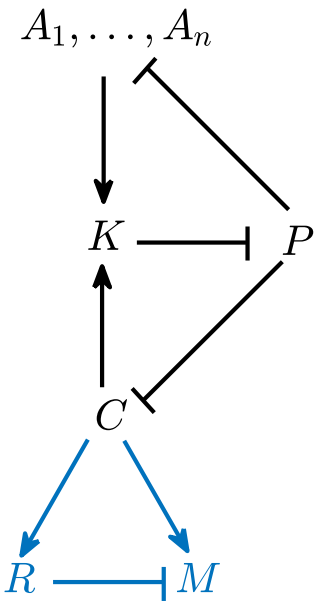

Figure 3: Schematic of the biochemistry model. We consider the black parts (biochemistry only) in Section 3.2, and add the blue parts (contractility) in Section 3.3. On the anterior half, A represents PAR-3 (in monomer and oligomer form), K represents the PAR-6/PKC-3 complex, and C represents CDC-42. The posterior PARs can be represented by a single protein species P.

realistic lifetimes on the order 5–20 s, the minimum flow speed to generate instability is about 40 μm/min, which is much faster than ever observed *in vivo*. Thus the dynamics of maintenance phase rescue are not due to myosin instabilities.[1]

3.2 Basic maintenance-phase biochemistry circuit

Because the dynamics of myosin alone are insufficient to generate instability, PAR proteins must be essential for rescue to occur [14]. We consequently introduce a model of maintenance phase biochemistry based on the diagram in Fig. 3, which in turn comes from [5, Fig. 2]. On the anterior side, we have three distinct protein species: PAR-3 (A), CDC-42 (C), and PAR-6/PKC-3 (K), each of which has a separate function. The posterior PARs (PAR-2, PAR-1, and CHIN-1) can be lumped into one species (denoted by P), which antagonizes both PAR-3 and CDC-42. The dimensional

[1]We note a distinction here between maintenance and establishment phase. In the latter, instabilities in the dynamics of rho combine with delayed negative feedback to yield pulsatile dynamics [11, 8, 7]. The connection between these pulsatile dynamics and the large-scale flows that establish polarity is still unknown.

equations which describe the circuit are

$$\partial_t A_1 = D_A \partial_x^2 A_1 + \left(k_A^{\text{on}} + k_A^+ f_A^+(A)\right) A_{\text{cyto}} - k_A^{\text{off}} A_1 \tag{2a}$$
$$+ 2k_A^{\text{dp}}(P)\hat{A}_2 - 2k_A^{\text{p}}\hat{A_1}^2 + \sum_{n=3}^{N}\left(A_n - k_A^{\text{dp}}(P)A_1 A_{n-1}\right)$$

$$\partial_t A_n = k_A^{\text{p}} A_1 (A_{n-1} - A_n) - k_A^{\text{dp}}(P)(A_n - A_{n+1}) \qquad N > n \geq 2 \tag{2b}$$

$$\partial_t A_N = k_A^{\text{p}} A_1 A_{N-1} - k_A^{\text{dp}}(P) A_N \tag{2c}$$

$$\partial_t C = D_C \partial_x^2 C + k_C^{\text{on}} C_{\text{cyto}} - k_C^{\text{off}} \left(1 + r_{\text{PC}} P\right) C \tag{2d}$$

$$\partial_t K = D_K \partial_x^2 K + r_{\text{ACK}} C \delta_{A>A_0} K_{\text{cyto}} - k_K^{\text{off}} K \tag{2e}$$

$$\partial_t P = D_P \partial_x^2 P + k_P^{\text{on}} P_{\text{cyto}} - k_P^{\text{off}} \left(1 + r_{\text{KP}} K\right) P \tag{2f}$$

The PAR-3 equations (2a)–(2c) describe the dynamics of PAR-3 oligomerization (an oligomer of size n denoted by A_n), for which we use the model developed in [4]. As discussed in detail there, the combination of oligomerization and positive feedback (through the term $k_A^+ f_A^+(A)$) imparts intrinsic bistability to the system. This bistability is strengthened when pPARs are included; through the term $k_A^{\text{dp}}(P)$, these posterior PARs promote depolymerization of PAR-3.

PAR-3 also gates the association of CDC-42 with PAR-6/PKC-3 (K), which is a complex that inhibits all posterior PARs [5]. To model this, we work off the observations in [12], which reveal that PAR-6/PKC-3 are recruited to the membrane by CDC-42, provided that there is a sufficient concentration (roughly 10% of the enriched anterior level) of PAR-3 on the membrane. Thus the total loading term in (2e) is proportional to the CDC-42 concentration times the cytoplasmic concentration of K, provided the PAR-3 concentration satisfies $A > A_0$. The other two equations (for CDC-42 and pPARs) are straightforward: we assume a basal rate of binding and unbinding, with an unbinding rate which is linearly enhanced by the inhibitor (pPARs for CDC-42 and PKC-3 for pPARs). In the supplemental appendix, we nondimensionalize (2), then use sets of existing experimental observations about the relative amount of each species on the anterior/posterior side of the embryo, as well as estimates of the amounts in the cortex vs. cytoplasm, to constrain the unknown parameters.

3.2.1 PAR proteins without contractility amplify asymmetries, but too slowly

In previous work on PAR-3 [4], we demonstrated that the diffusion of the smaller oligomer sizes (monomers in our model) sets a unique boundary position. In Fig. 4, we demonstrate that this

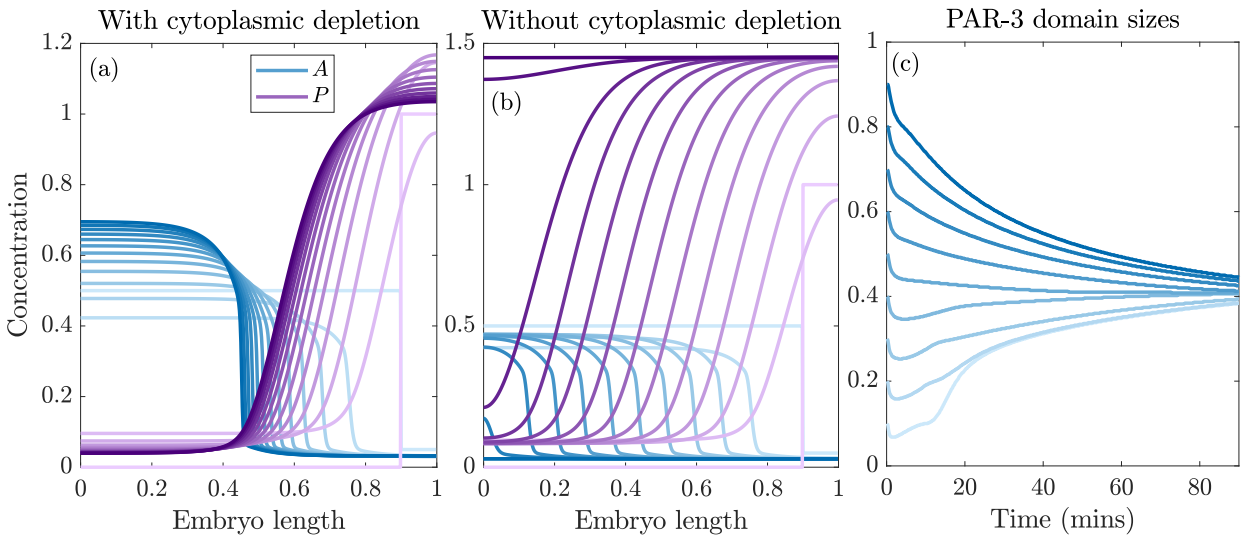

Figure 4: The biochemistry model (2) has a unique boundary position controlled by cytoplasmic depletion, which can only be achieved in realistic timescales if started near the equilibrium position. We simulate the progression of initially separated aPAR/pPAR domains. (a) 90% initial PAR-3 domain size with cytoplasmic depletion. (b) 90% initial PAR-3 domain size *without* cytoplasmic depletion after $t = 10$ mins. A sequence of 13 time points from $t = 0$ (lightest colors) to $t = 120$ mins (darkest colors) is shown. (c) PAR-3 domain size (length where the PAR-3 concentration is 80% of the maximum or larger) over time starting from varied initial conditions.

with the full biochemistry by simulating the contraction of a PAR-3 domain that initially takes up 90% of the embryo. The boundary shifts because a high concentration of pPARs shifts the local equilibrium of PAR-3 oligomerization towards the monomer state, which makes bistability impossible [4]. Consequently, we observe contraction of the PAR-3 domain, with a peak that grows over time, and expansion of the PAR-2 domain, both of which eventually reach a steady state. The concentration of PAR-2 at the edge of the domain decreases over time, which suggests that cytoplasmic depletion might be responsible for pinning the boundary. To demonstrate that a fixed pool of protein is key to arresting posterior domain expansion, in the right panel of Fig. 4 we simulate with a cytoplasmic pool that is "frozen" at its value at $t = 10$ mins. The result is an anterior domain which shrinks at a constant rate with constant peak concentration, and a posterior domain which expands at a constant rate with the same concentration at the edge. Given enough time, the posterior domain invades the entire embryo length.

In [4], we showed that the diffusion-controlled shift of the PAR-3 boundary occurs on timescales of hours, meaning that the boundary never reaches a steady position in practice. This is confirmed in Fig. 4, which shows that cytoplasmic depletion can only act rapidly to stop boundary progression if the initial boundary size is close to the steady state. The simulation in Fig. 4(a), which starts at 90% PAR-3 enrichment takes some two hours to reach the steady state; while a simulation starting at 50% PAR-3 enrichment takes only 5–10 minutes. In order to reproduce rescue, we need to introduce cortical flows that initially shift the boundary at a faster initial rate. If these cortial flows are then arrested, cytoplasmic depletion can then prevent the boundary from shifting, leading to a steady state.

3.3 Coupling contractility to biochemistry reproduces initial stages of rescue

Because neither myosins nor PAR proteins can rescue maintenance phase asymmetries by themselves, there must be an interaction with PAR proteins that amplifies gradients in contractility to rescue the correct polarized state. To account for this, we add the myosin dynamics (1) to the biochemistry system (2). In doing this, we also incorporate advective terms that ensure that each protein moves with the local cortical velocity [3], and make CDC-42 a promoter of myosin. The equations corresponding to this situation are a straightforward extension of (1) and (2), and we therefore confine them to the supplemental material, where we give a non-dimensional version and fit the unknown parameters.

In Figure 5 shows the results when we the parameters to match the experimentally-measured

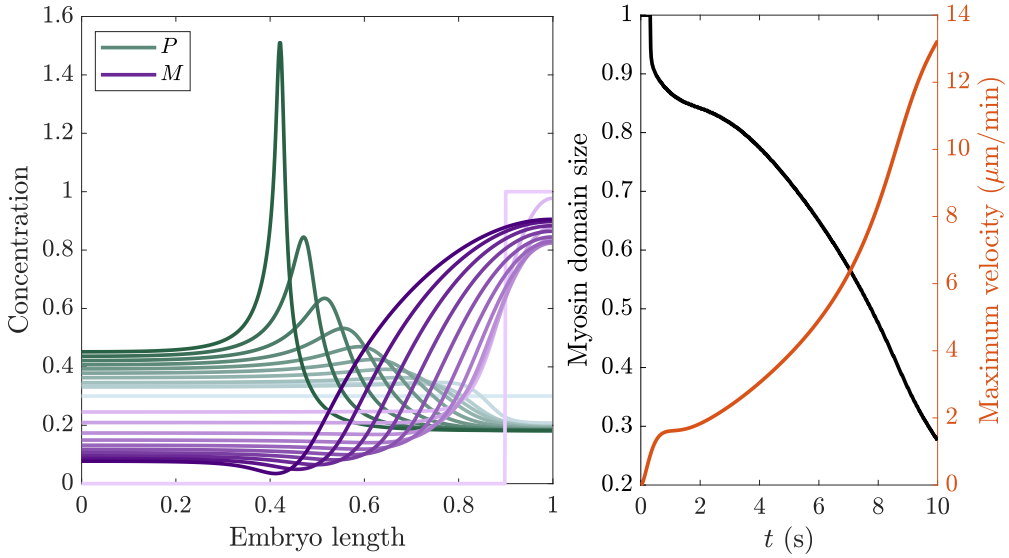

Figure 5: Simulating rescue with a coupled model of contractility and biochemistry. Left panel: time course of rescue, with lines shown at equal time points from $t = 0$ to $t = 7.5$ mins (intervals of 45 seconds). The green and purple lines show pPARs (P) and myosin (M), respectively. Right panel: the myosin domain size (proportion of the domain with concentration > 0.25) over time (black curve, left axis) and the corresponding flow speed (red curve, right axis).

initial speeds of rescue. The left panel shows the dynamics of the simulation from $t = 0$ (lightest colors) to $t = 7.5$ mins (darkest colors), while the right panel shows the myosin boundary position (0 is the anterior pole, 1 is the posterior pole) and the flow speeds over time. Our statistics show the beginning of the rescue process, where an initially peaked profile of PAR-2 invades the anterior domain, concentrating anterior PARs in the middle and thereby increasing the concentration of pPARs in the posterior. As a result of this, CDC-42 gets inhibited in the posterior, which gives a gradient of myosin from posterior to anterior. The gradient of myosin generates a flow which further compacts the anterior domain. The timescale of this compaction is much faster than without flows (Fig. 4), and indeed occurs on a timescale of minutes and not hours.

While our model reproduces the initial stages of the rescue process, there is no mechanism in it to halt the advancing myosin front. With the correct model parameters, the tendency of flow to concentrate the aPARs overwhelms the effect of cytoplasmic depletion (which tends to slow the boundary motion). As a result, the boundary contracts with nothing to slow it down. Indeed, in the limit as time goes to infinity, we expect one peak of aPARs and myosin at the anterior pole, which is in sharp contrast to our experimental result which showed a sharp drop in the anterior-directed

flow speed in the late stages of maintenance phase (see inset of Fig. 1).

4 Branched actin as a brake on contractility

Our modeling so far identified two regimes of behavior, depending on the sensitivity of myosin to the CDC-42 concentration. Roughly speaking, if CDC-42 promotes myosin at a rate much smaller than the basal rate (0 in Fig. 4), the cytoplasmic dynamics are sufficient to stop the pPARs from invading too far into the anterior domain. But this model has to be discarded because the dynamics occur over unrealistically long timescales. To match the speed of rescue, CDC-42 has to promote myosin at a rate much larger than the basal rate, which leads to fast flows and (in this model) a rapid concentration of the anterior domain into a peaked profile at the anterior pole (Fig. 5). Thus, we are missing an important interaction that slows down the advancing myosin peak, rapidly dropping the flow speed and allowing cytoplasmic depletion to pin the boundary. This interaction is the focus of this section.

4.1 Experiments in arx-2 (RNAi) embryos establish a hyper-contractile state

Figure we want to make for this section:

(a) Pictures of wild-type vs. arx-2 (RNAi) embryos in late maintenance
(b) Measurements of myosin peak in maintenance (left panel of Fig. 6; put flows in SI if at all)
(c) Pictures of ect-2 (ts) with and without arx-2 (RNAi) in early and late maintenance
(d) Kymograph of rescue with and without arx-2 (RNAi)
(e) Pictures of control vs. arx-2 (RNAi) for embryos *with nocodozole* treatment
(f) Myosin intensity & flow in control vs. arx-2 (RNAi) *with nocodozole* (Fig. 7 here)

We hypothesize that branched actin might stop the anterior cap from becoming hyper-contractile. To test this hypothesis, we deplete wild type embryos of arx-2, a protein which activates the arp 2/3 complex and the assembly of branched actin. Figure 6 shows the average myosin intensity and flow profiles over the last three minutes of maintenance phase in wild-type (red) and arx-2 (RNAi) treated embryos (blue). While the wild-type intensity seems to be roughly stalled at a boundary position 40% of the embryo length, the arx-2 (RNAi) embryos demonstrate hyper-contractility, with a myosin peak that shifts to the anterior (and increases) over time.

The flow measurements in *arx-2* (RNAi) embryos are chaotic and noisy because the hyper-contractile anterior cap is not always positioned directly on the anterior pole, so flows can be generated off the A/P axis. In Fig. 6, we show the average flow speeds in embryos where the

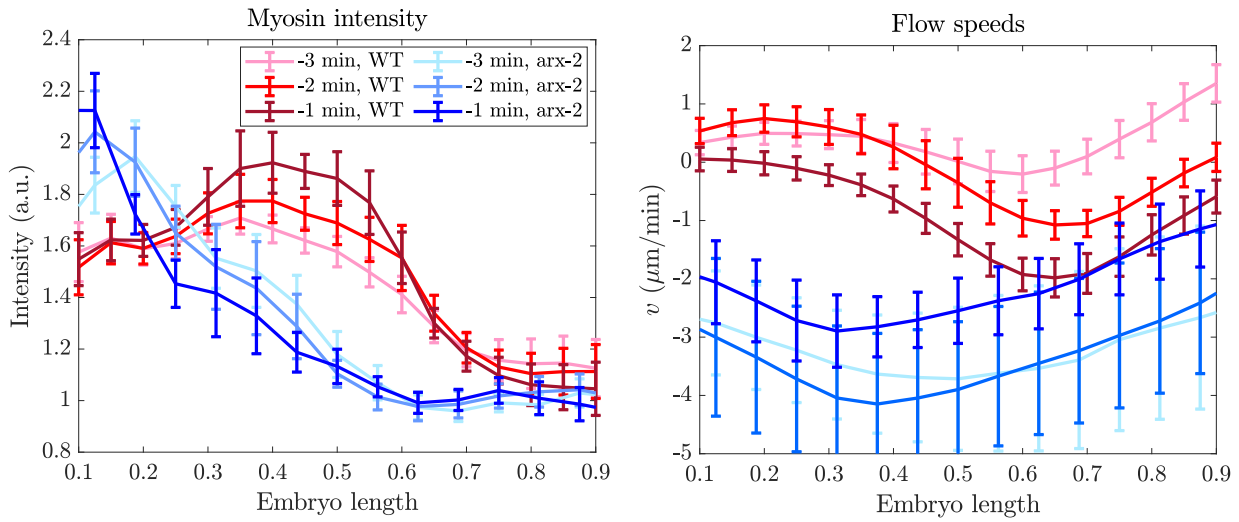

Figure 6: Comparing late maintenance phase in wild-type (red lines) and arx-2 (RNAi) treated embryos (blue lines). The lightest colors show the average profile between 2 and 3 minutes prior to cytokinesis onset, the middle colors between 1 and 2 minutes, and the darkest colors show the profile in the last minute of maintenance phase. Left plot: the myosin intensity profile ($n = 12$ for *arx-2*). Right plot: flow speeds ($n = 6$ for *arx-2*, discarding embryos that do not have A/P axis flows).

A/P flow dominates other directions (6 of the 12 embryos). These flows have a maximum speed around 2.5–4 μm/min. Unlike the wild-type profile, whose point of maximum flow and stall point are roughly constant in time, the *arx-2* (RNAi) flow profiles show no stall point, are larger in magnitude, and have a local maximum whch is positioned far to the anterior of the wild-type.

We hypothesized that the chaotic and noisy flow speeds in *arx-2* (RNAi) embryos were a result of the smaller anterior cap being pulled and pushed around by forces from the mitotic spindle. Because of this, we applied nocodazole, a drug which depolymerizes microtubules, and observed the resulting dynamics. Interestingly, nocodazole treatment of wild type embryos appears to remove the posterior-directed flow earlier in early maintenance phase (Fig. 6) [12]. In late maintenance, however, the dynamics are relatively unchanged with nocodazole treatment, with a peak in the myosin concentration around 40% embryo length and a maximum flow speed of 2 μm/min at 60% embryo length (blue lines in Fig. 7).

In *arx-2* (RNAi) embryos, nocodazole treatment significantly improved the patterns of flow, confining them to the A/P axis and allowing us to extract meaningful information. Similar to the case without nocodazole, embryos treated with arx-2 (RNAi) and nocodazole showed a hypercontractile anterior myosin cap (Fig. 7), with the cap continuing to contract over time to the very

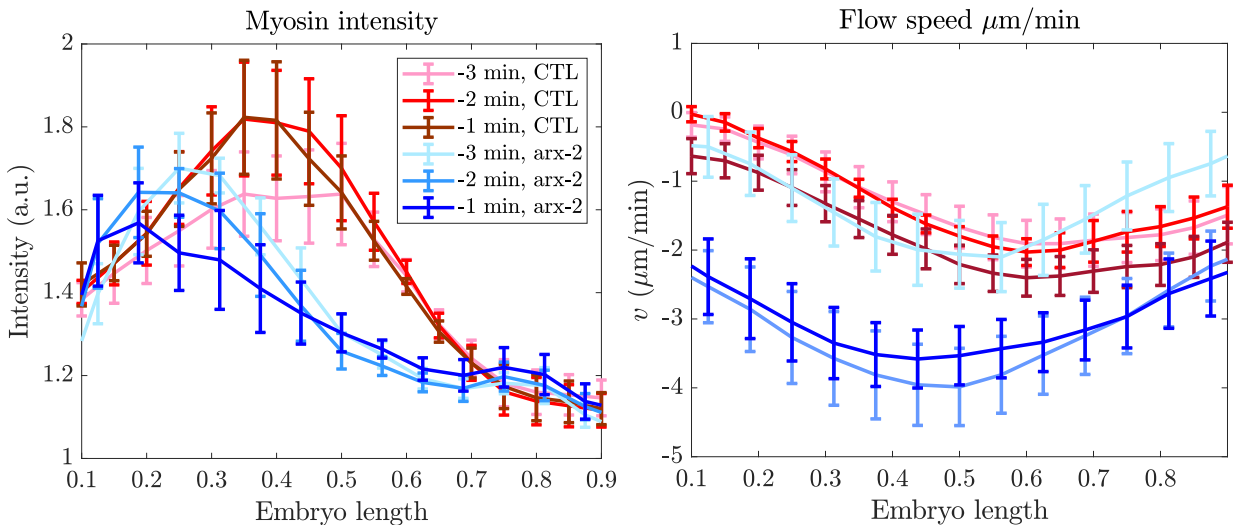

Figure 7: Comparing late maintenance phase in wild-type (red lines) and arx-2 (RNAi) treated embryos (blue lines) *with nocodazole treatment*. The lightest colors show the average profile between 2 and 3 minutes prior to cytokinesis onset, the middle colors between 1 and 2 minutes, and the darkest colors show the profile in the last minute of maintenance phase. Left plot: the myosin intensity profile. Right plot: flow speeds.

edge of the anterior domain. The contraction of the cap corresponded with marked increases in flow speed during maintenance, so that flows went from 1.5 μm/min during the third minute before anaphase onset to 3–4 μm/min, with the point of maximum flow occuring at 40% embryo length instead of 60% (Fig. 7). Thus, regardless of the presence of microtubules, depletion of arx-2 by RNAi leads to a hypercontractile state with a larger velocity and a cap which tends to fall of the edge of the embryo, similar to what we observed in simulations in Fig. 5. We now propose a model for how branched actin could inhibit contractility and lead to the formation of a stable boundary.

4.2 Model of branched actin

Figure we want to make for this section:

(a) Schematic showing ways we consider branched actin working
(b) Simulation with tension reduction showing boundary stops (and remaining issues; Fig. 8 here)
(c) "Best" simulation reproducing all trends (Fig. 9 here).

To model branched actin, we work off the following two important observations from our maintenance-phase rescue experiments: first, the pinning of the myosin domain and drop in velocity happen quite abruptly, and second, the rapid drop in velocity is *not* accompanied by strong changes in the myosin concentration profile (Fig. 1). These observations together suggest that there is an ultra-sensitive dependence of contractility (not myosin concentration) on branched actin. As rescue

progresses, branched actin becomes active on the anterior, providing a "brake" which slows down contractility and progression of the boundary.

To translate our hypothesis into our model, we make the following assumptions,

1. To activate branched actin, we assume a threshold of CDC-42 above which branched actin is created. The threshold is reached roughly when the A/P boundary reaches the middle of the cell.

2. Branched actin assembly is autocatalytic, since new branches become sites for additional branches.

3. Branched actin unbinds from the cortex with characteristic rate k_R^{off} (about 8 s lifetime).

4. While branched actin does not diffuse in the cortex, polymerization of actin leads to a spreading out of the branched network, and so we include nonzero diffusivity.

5. Branched actin inhibits contractility.

The first four assumptions lead to the advection-diffusion-reaction equation

$$\partial_t R + \partial_x(vR) = D_R \partial_x^2 R + \left(r_{\text{CR}} \max\left(C - C_R, 0\right) + r_{\text{RR}} R\right) R_{\text{cyto}} - k_R^{\text{off}} R \tag{3a}$$

for the evolution of branched actin (R) in time and space. For the fifth assumption, we postulate a simple relationship for how branched actin impacts contractile stress

$$\sigma_a = \frac{\sigma_0 M}{1 + r_{\text{R}\sigma} R}. \tag{3b}$$

We use division of the stress instead of subtraction because, as the branched actin concentration goes to infinity, we expect the tension to approach zero, as was shown to be the case *in vitro* using laser ablation [10]. In the SI, we give the dimensionless form of (3a) and (3b) and estimate the unknown parameters.

The dynamics of rescue in this case are shown in Fig. 8. In the early stages of rescue, we see a concentration of myosin and CDC-42 into an interior peak which grows over time. Once the concentration of CDC-42 at the peak exceeds the threshold $C_R = 0.25$, branched actin is produced. This causes an immediate drop in contractility within the peak (see the active stress profile at intermediate times), which leads to a leveling out of the anterior profiles of CDC-42 and myosin (weaker flows in the anterior allow CDC-42 to diffuse over). Following this, branched actin builds up

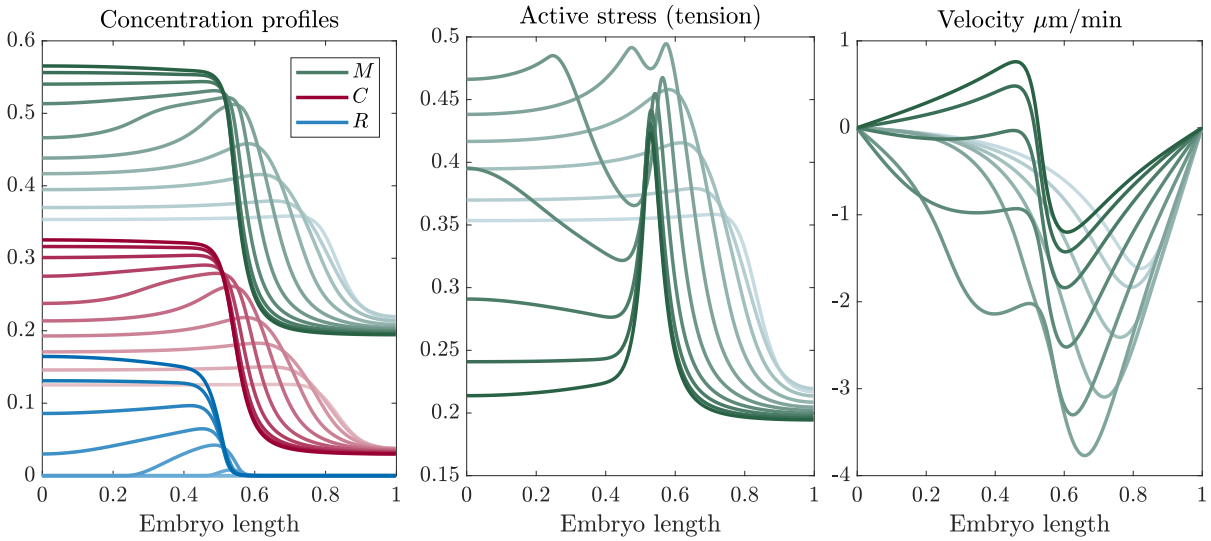

Figure 8: Dynamics of rescue when branched actin inhibits stress/tension according to (3b). The left panel shows the concentration profile of myosin (M, green), CDC-42 (C, red), and branched actin (R, blue) over time. The middle panel shows the active stress (tension), normalized by σ_0, and the right panel shows the velocity in units of μm/min. Each panel has a series of ten lines which show the profile at $t = 1, 2, \ldots 10$ min, with darker lines showing later times.

on the anterior. The boundary stops moving when the tension on the anterior balances the tension on the posterior, leaving an intermediate zone of contractility at around 60% embryo length.

While these simulations qualitatively reproduce what we observe in maintenance phase rescue (the anterior boundary progresses and then stops), there are two details that do not match the experiments. First, as soon as branched actin inhibits contractility, the myosin concentration profile tends to flatten out in the anterior (it is no longer peaked). This is not what we see in the rescue experiments (data in Fig. 1), where myosin stays peaked after the boundary stops moving. Second, the flow profile from simulations is symmetric about the myosin peak with a flow of about 1 μm/min coming from *both* the anterior and posterior into the zone of contractility. This is also not what we observe in experiments, where the flow profile is essentially flat in the anterior (up to 40% embryo length), and anterior-directed in the posterior (see Fig. 1). In the following sections, we add to our model to try to address these two issues.

4.2.1 Detail 1: reproducing the myosin profile

Let us consider first the issue of the myosin concentration profile. What is missing from our inhibition model that causes myosin to be flat in the anterior? We previously saw that inhibition

of tension by branched actin inhibits flows in the anterior, which allows diffusion to level out the anterior CDC-42 profile, which in turn levels out the anterior myosin profile. At steady state, there is a compressive flow in the middle of the embryo, but the speed of the flow (at most 2 μm/min as measured in experiments) is insufficient to concentrate myosin or CDC-42. Some statement about myosin and CDC-42 distributions.

We propose two possible explanations to address this issue. First, a simple explanation is that myosin could have a longer lifetime than 8 s, as we can track the large clusters for some 30 s before they disappear. A second possibility is that branched actin could also inhibit myosin directly in the anterior, for example by thickening the cortex and forcing myosin unbinding (which was shown to occur in mouse oocytes [2]). As shown in the SI, both of these models show a better fit to the data as far as the myosin profile, but neither have a velocity which matches that obtained from experiments, as there is still a backflow in the anterior which results from the reduction of tension and myosin inhibition.

4.2.2 Detail 2: reproducing the (lack of) flow on the anterior

Because there is an enrichment of myosin at the midline relative to the anterior pole, and because branched actin inhibits tension, the results in Fig. 8 show an anterior gradient in tension and a flow from the anterior to the midline. However, in wild-type and *ect-2* (ts) embryos in late maintenance, we never detect a substantial (larger than 1 μm/min) flow in the anterior (see Fig. 1), despite the gradient in myosin (and presumably in tension). Put another way, gradients in tension do not translate to flows the same way in the anterior as they do in the posterior, presumably because of branched actin.

Our model equation for velocity (1b) has two addition parameters that model how flow responds to changes in contractility. The parameter that controls the magnitude of the flow obtained for a fixed tension gradient is the drag or friction coefficient γ, and the parameter that controls the response to a given rate of strain ($\partial_x v$) is η. We propose that branched actin could modulate each of these parameters according to the linear relationships

$$\gamma(R) = \gamma_0 \left(1 + r_{\mathrm{R}\gamma} R\right) \qquad \eta(R) = \eta_0 \left(1 + r_{\mathrm{R}\eta} R\right).$$

These two models, while superficially similar, are at a deeper level quite different. In the case of increased friction, we are proposing that the velocity can rapidly change from negative (in the posterior) to positive (in the anterior), but that the magnitude of the positive velocity in the anterior

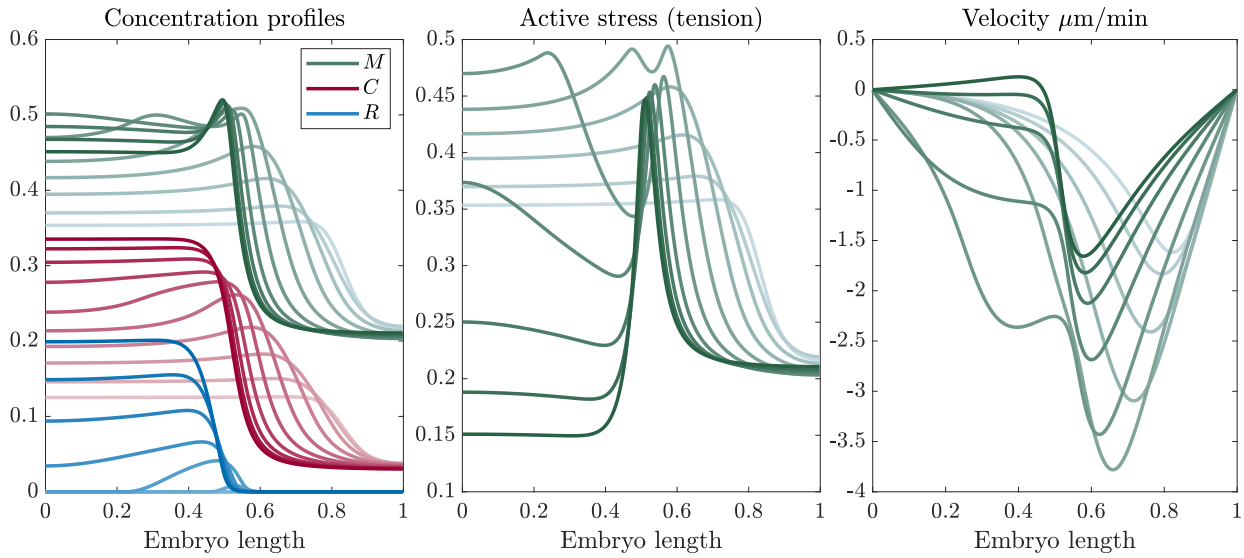

Figure 9: Dynamics of rescue when branched actin inhibits stress, directly inhibits myosin, and enhances viscosity. The left panel shows the concentration profile of myosin (M, green), CDC-42 (C, red), and branched actin (R, blue) over time. The middle panel shows the active stress (tension), normalized by σ_0, and the right panel shows the velocity in units of μm/min. Each panel has a series of ten lines which show the profile at $t = 1, 2, \ldots 10$ min, with darker lines showing later times.

is necessarily smaller because the same force on that side generates a smaller velocity than on the posterior. Increased viscosity, by contrast, says that the branched actin network resists changes in strain rate (sharp changes in velocity). By increasing viscosity, we are proposing that the changes in tension on the anterior side cannot induce compressive flows because of viscous resistance.

In the SI, we analyze both of these models, and conclude that either a moderate increase (a factor of 2) in the viscous resistance, or a large increase in the frictional resistance (a factor of 10) in the anterior is sufficient to reproduce the dynamics observed experimentally. A large increase in viscosity results in an anterior flow that cannot rapidly respond to changes in tension, and as such cannot stop the boundary from progressing by slowing the flow. A small increase in friction is simply not large enough to reproduce the experimental flow profile (it still retains the compressive flow in the anterior).

4.2.3 Best case parameters

Our best attempt to reproduce the experimental data is shown in Fig. 9. In this simulation, we add direct inhibition of myosin by branched actin, so that branched actin in the anterior increases the off rate by about 50%. Likewise, we add a viscosity enhancement, so that the viscous resistance in

the anterior (with branched actin) is roughly 3 times the posterior (see SI for exact parameters). The dynamics in Fig. 9 (myosin and flow profiles) agree well with those observed experimentally,

5 Discussion

References

[1] Justin S Bois, Frank Jülicher, and Stephan W Grill. Pattern formation in active fluids. *Biophysical Journal*, 100(3):445a, 2011.

[2] Agathe Chaigne, Clément Campillo, Nir S Gov, Raphaël Voituriez, C Sykes, Marie-Hélène Verlhac, and Marie-Emilie Terret. A narrow window of cortical tension guides asymmetric spindle positioning in the mouse oocyte. *Nature communications*, 6(1):6027, 2015.

[3] Rukshala Illukkumbura, Nisha Hirani, Joana Borrego-Pinto, Tom Bland, KangBo Ng, Lars Hubatsch, Jessica McQuade, Robert G Endres, and Nathan W Goehring. Design principles for selective polarization of par proteins by cortical flows. *Journal of Cell Biology*, 222(8), 2023.

[4] Charles F Lang, Alexander Anneken, and Edwin Munro. Oligomerization and feedback on membrane recruitment stabilize par-3 asymmetries in c. elegans zygotes. *bioRxiv*, pages 2023–08, 2023.

[5] Charles F Lang and Edwin Munro. The par proteins: from molecular circuits to dynamic self-stabilizing cell polarity. *Development*, 144(19):3405–3416, 2017.

[6] Mirjam Mayer, Martin Depken, Justin S Bois, Frank Jülicher, and Stephan W Grill. Anisotropies in cortical tension reveal the physical basis of polarizing cortical flows. *Nature*, 467(7315):617–621, 2010.

[7] Ani Michaud, Marcin Leda, Zachary T Swider, Songeun Kim, Jiaye He, Jennifer Landino, Jenna R Valley, Jan Huisken, Andrew B Goryachev, George von Dassow, et al. A versatile cortical pattern-forming circuit based on rho, f-actin, ect2, and rga-3/4. *Journal of Cell Biology*, 221(8):e202203017, 2022.

[8] Jonathan B Michaux, François B Robin, William M McFadden, and Edwin M Munro. Excitable rhoa dynamics drive pulsed contractions in the early c. elegans embryo. *Journal of Cell Biology*, 217(12):4230–4252, 2018.

[9] Edwin Munro, Jeremy Nance, and James R Priess. Cortical flows powered by asymmetrical contraction transport par proteins to establish and maintain anterior-posterior polarity in the early c. elegans embryo. *Developmental cell*, 7(3):413–424, 2004.

[10] Camelia G Muresan, Zachary Gao Sun, Vikrant Yadav, A Pasha Tabatabai, Laura Lanier, June Hyung Kim, Taeyoon Kim, and Michael P Murrell. F-actin architecture determines constraints on myosin thick filament motion. *Nature communications*, 13(1):7008, 2022.

[11] Masatoshi Nishikawa, Sundar Ram Naganathan, Frank Jülicher, and Stephan W Grill. Controlling contractile instabilities in the actomyosin cortex. *Elife*, 6:e19595, 2017.

[12] Anne Sailer, Alexander Anneken, Younan Li, Sam Lee, and Edwin Munro. Dynamic opposition of clustered proteins stabilizes cortical polarity in the c. elegans zygote. *Developmental cell*, 35(1):131–142, 2015.

[13] Yu Chung Tse, Michael Werner, Katrina M Longhini, Jean-Claude Labbe, Bob Goldstein, and Michael Glotzer. Rhoa activation during polarization and cytokinesis of the early caenorhabditis elegans embryo is differentially dependent on nop-1 and cyk-4. *Molecular biology of the cell*, 23(20):4020–4031, 2012.

[14] Seth Zonies, Fumio Motegi, Yingsong Hao, and Geraldine Seydoux. Symmetry breaking and polarization of the c. elegans zygote by the polarity protein par-2. *Development*, 137(10):1669–1677, 2010.